Plasma Sci. Technol. **25** (2023) 055104 (6pp) https://doi.org/10.1088/2058-6272/acafc2

Initial testing of ohmic heating through double flux swing during electron cyclotron start-up in the QUEST spherical tokamak

Yifan ZHANG (张逸凡)[1,*], Takumi ONCHI[2], Kazuo NAKAMURA[2], Qilin YUE (岳其霖)[1], Takahiro NAGATA[2], Shoji KAWASAKI[2], Kengoh KURODA[2], Makoto HASEGAWA[2], Ryuya IKEZOE[2], Takeshi IDO[2], Kazuaki HANADA[2] and Hiroshi IDEI[2]

[1] Interdisciplinary Graduate School of Engineering Sciences, Kyushu University, Kasuga 816-8580, Japan
[2] Research Institute for Applied Mechanics, Kyushu University, Kasuga 816-8580, Japan

E-mail: y.zhang@triam.kyushu-u.ac.jp

Received 28 July 2022, revised 29 December 2022
Accepted for publication 3 January 2023
Published 21 February 2023

Abstract

A power-supply system was developed for Ohmic heating (OH) to double $\times 10^{18}$ the amount of change magnetic flux in the primary central solenoid (CS) on the QUEST spherical tokamak. Two power supplies are connected with stacks of insulated-gate bipolar transistors, and sequentially operated to generate positive and negative CS currents. This bipolar power-supply system is controlled via a field-programmable gate array, which guarantees the safety of the entire system operation. The new OH system, assisted by electron cyclotron heating, enables the stable generation of plasma currents exceeding 100 kA. Moreover, the achieved electron density over the wide range in the major radial direction exceeds the cut-off density for one of the high-power microwave sources in QUEST. This strategy yields target plasmas for future experiments with the electron Bernstein wave.

Keywords: spherical tokamak, ohmic heating, electron cyclotron heating, FPGA

(Some figures may appear in colour only in the online journal)

1. Introduction

The initiation of tokamak plasmas under different heating scenarios has been explored through radio-frequency heating [1, 2] and neutral beam injection [3, 4]. As a fundamental technique, Ohmic heating (OH) has emerged as an effective method to start up the plasma currents in tokamaks [5, 6]. Since the inception of tokamak research, central solenoid (CS) coils featuring an iron core have been employed to apply high toroidal-loop voltages. To save on the central space and improve the cost-effectiveness, modern tokamak designs tend to incorporate air-core coils as the CS. If the CS coils are manufactured using superconductive materials, the application of low loop voltages to the toroidal plasma is rendered feasible.

In particular, the CS space required for a spherical tokamak is less than that for conventional tokamaks; hence, air-core coils with reduced volt-seconds are installed as the CS. To overcome this limitation, which focuses on spherical tokamak, current start-up methods to reduce the dependence on OH have been established. From this perspective, co-axial helicity injection (CHI) [7–9], local helicity injection (LHI) [10], and plasma merging [11] have accomplished effective results in achieving plasma current start-up. As these methods consume high levels of power transiently, they result in the generation of high-density plasmas. In particular, radio-frequency heating is advantageous for maintaining the tokamak equilibrium across a longer time scale than the transient methods. Experiments with lower hybrid resonance heating and electron cyclotronheating (ECH) have verified that energetic electrons play an essential role in initiating non-inductive plasma [12].

* Author to whom any correspondence should be addressed.

A combination of OH and other heating methods would be the fundamental scenario to generate plasmas stably in advanced spherical tokamaks [13, 14]. ECH is established as the main heating source in the QUEST spherical tokamak [15–17]. In a previous experiment using a single flux swing, the plasma current reached 100 kA [12]. With a higher plasma current, a higher electron density could be achieved efficiently. Under the condition that the electron density exceeds the cut-off density for the EC wave, the electron Bernstein wave (EBW) transformed from the EC waves can be excited, thereby heating of the over-dense plasmas [18]. Notably, a steady-state heating and current-drive experiment is planned for the QUEST project using an 8.56 GHz EC-heating system with 250 kW RF power [19]. Additionally, this heating system is used for EBW experiments. Although energetic electrons are generated through RF start-up, the EBW heats bulk electrons. In this regard, a high-density discharge through CHI or LHI may help prevent the initiation of an excessive number of energetic electrons.

A target plasma is required to conduct an experiment on the heating and current-drive via EBW in QUEST. If the electron density exceeds $n_e > 9.1 \times 10^{17}\ \mathrm{m}^{-3}$ over the wide range in the major radial direction, the plasma can be rendered overly dense for an 8. 56 GHz EC wave. Our approach is based on enhancing the OH by doubling the flux swing [20]. Two high-power current sources are combined using two switches comprising 2×2 insulated-gate bipolar transistor (IGBT) stacks and a diode stack. Accordingly, a high-power bipolar power supply is connected to the CS to achieve OH in QUEST. Furthermore, to validate the effectiveness of this upgrade, the double flux swing is applied to the EC-heated tokamak in this experiment.

The remainder of this paper is organized as follows. The design of the new OH system is introduced in section 2. This section presents a conceptual circuit, a current start-up scenario, and a control system of the OH system. An interlock system based on a field programmable gate array (FPGA) is designed to protect the upgraded OH system. Section 3 illustrates the experimental results corresponding to the non-inductive and inductive current start-ups. Finally, the conclusions are drawn in section 4.

2. Ohmic heating system

2.1. Power supply system

The power supply system is established to flexibly energize the CS coil. The CS coil is located in the center of the QUEST consisting of three coils, named PF4-1, PF4-2, and PF4-3, in series. PF4-1 and PF4-3 each has 72 turns and PF4-2 has 144 turns. In OH experiment, the total number of turns is 216 with PF4-1, PF4-3, and half of PF4-2 connected in series PF4-1 and PF4-3, suited on the top and bottom. Each has a radius of 163 mm and length of 590 mm, while PF4-2 in the middle, has a radius of 172 m and length of 792 mm. The CS coil can be considered as a combination of an inductance, $L_{CS} = 1.88$ mH, and a resistance, $R_{cs} = 30$ m Ω, in series; both circuit parameters are experimentally measured quantities. An inductance, L_p, and a resistance, R_p, of the plasma comprise a plasma circuit loop. The transformer is equivalent to a T-type transformer, as illustrated in figure 1, where the self-inductances are $L_1 = L_{cs} - L_M$, and $L_2 = L_P - L_M$. Here, L_M (=8 μH) represents the mutual inductance between the CS loop and the plasma loop.

The two DC power supplies, the positive supply (PS) and negative supply (NS), are powered by three-phase ACs through the control of six thyristor stacks. Using both the PS and NS power supplies, bipolar voltages can be applied to the CS coil, provided as they are seamlessly controlled. Additionally, the two IGBT stacks installed between the power supplies and the CS coil function as switches.

The bipolar power supply is controlled by the QUEST Central Control System (QCCS), while the IGBT stacks are controlled by the IGBT control system, which mainly comprises the FPGA, isolation amplifiers, transmitters, and receivers. The IGBT gate signals, transmitted by the FPGA, are used to switch on/off the IGBTs. These signals are transferred by transmitters and receivers through light cables to the IGBT drivers. Accordingly, an equivalent circuit is established, as illustrated in figure 1. T_1 in figure 1 denotes a conceptual trigger component of the 'on' signal that mimics a plasma breakdown in this equivalent circuit. This component is used in the simulations, as described in the subsequent sections.

L_p and R_p are calculated using the following equations [21]:

$$L_p = \mu_0 R\left(\ln\frac{8R}{a} + \frac{l_i}{2} - 2\right), \tag{1}$$

$$R_p = \left(\frac{1}{en_e}\cdot\frac{\nu_{ei}}{e}\right)\frac{2\pi R}{\pi a^2} = \eta\frac{2\pi R}{\pi a^2}, \tag{2}$$

where the major radius is denoted by R, the minor radius is symbolized by a, and internal inductance values l_i. Their values respectively are $R = 0.64$ m, $a = 0.40$ m, and $l_i = \frac{11}{12}$ for a typical tokamak equilibrium in QUEST. ν_{ei} indicates the electron–ion collision frequency, and η denotes the resistivity of hydrogen plasma, which is expressed as

$$\eta = \left(\frac{m_e}{en_e}\cdot\frac{\nu_{ei}}{e}\right) = \frac{1.65\times10^{-9}\times Z_{eff}\times\ln\Lambda}{T_e^{\frac{3}{2}}}, \tag{3}$$

where Coulomb logarithm $\ln\Lambda = 17$ and $Z_{eff} = 1$, as the effective nuclear charge. Particularly, the plasma resistance is affected by the electron temperature T_e.

As shown by the arrows depicted in figure 1, the operation controlling PS and NS in OH is conducted in two periods. In the first period, the PS and IGBT stack 1 are turned on, and the current in the CS loop flows clockwise, as indicated by the red arrow. Conversely, in the second period, the PS and IGBT stack 1 are turned off, and the NS and IGBT stack 2 are subsequently turned on. In this case, the CS current flows through IGBT 2 and NS counterclockwise, as shown by the blue arrows.

The equivalent circuit is simulated using a power electronics simulator (PSIM; Powersim Inc.), as indicated in

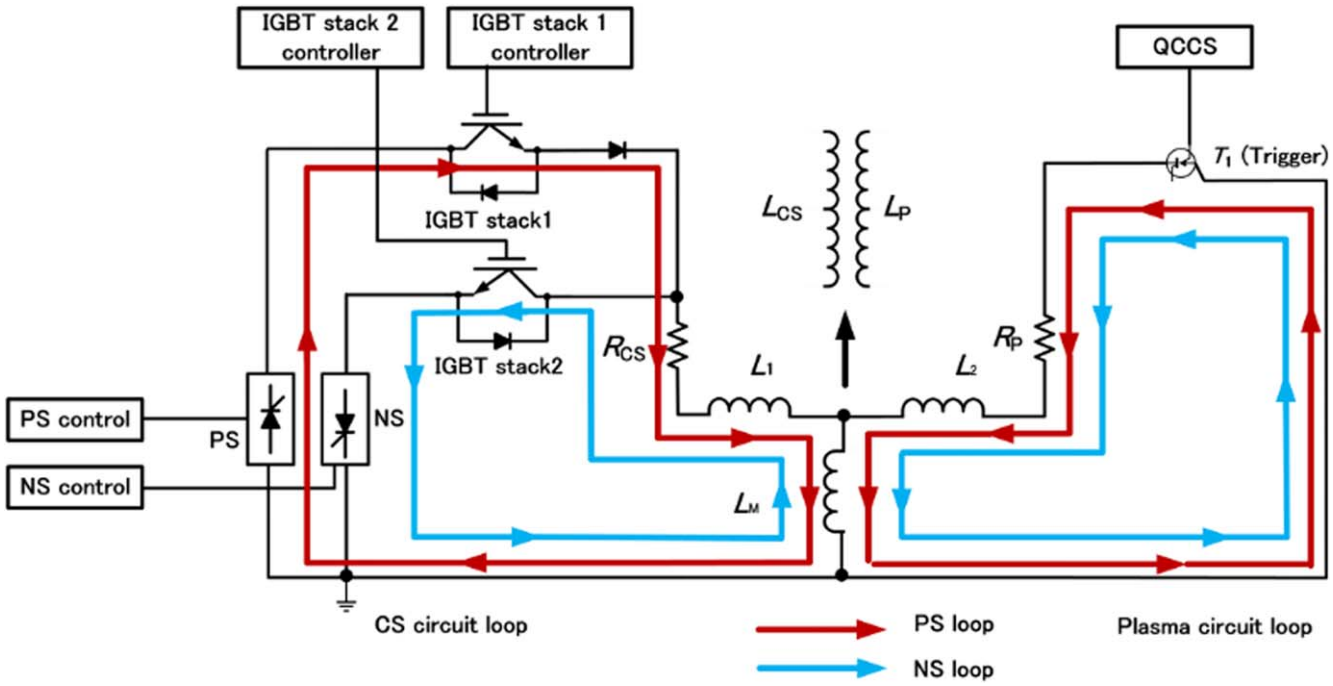

Figure 1. Equivalent circuit for OH power supply. PS current loop through the power supply, IGBT stack 1, and CS coil on the primary side is represented by the red arrow. On the secondary side, plasma current flows as shown by ramping down primary side current. NS current loop through the power supply, IGBT stack 2, and CS coil on the primary side is indicated by the blue arrow. On the secondary side, plasma current flows by ramping down primary side current. The transformer is equivalent to a T-type circuit consisting of self-inductance L_1 and L_2 and mutual inductance L_M between primary and secondary sides.

figure 2. The plasma resistance decreases with increasing temperature. Considering both the thermal and energetic electrons, R_p is set in the range from 200 to 2 $\mu\Omega$.

The PS and NS supply negative and positive voltages in this circuit setup. On applying −375 V to the CS, the current can increase to 8 kA. A loop voltage through the first swing is supplied as the current rapidly decreases to 0 A. Furthermore, the plasma current starts increasing, following the working principle of the transformer; it increases up to 60 kA at 2.52 s. The NS provides a voltage of up to 375 V to the CS coil, and the current increases to 8 kA from 2.52 to 2.62 s. Finally, the plasma current attains a maximum value of approximately 120 kA through a double flux swing.

2.2. Interlock system

As the maximum CS current reaches 8 kA during the OH operation, this working condition entails a risk of damage to the power-supply if the IGBT stacks are not appropriately controlled. For example, the current via the PS may flow through IGBT stack 2 to the closed circuit with NS if both IGBT stacks 1 and 2 are turned on simultaneously. Therefore, to protect the circuit components and power supplies, an interlock system was designed using an FPGA configuration; this system detects the IGBT signals and yields enabling signals for the power supplies and IGBT stacks.

This FPGA interlock system comprises two parts:

(1) Timer

The logical control of the PS timer, utilized to control and drive other FPGA interlock signals, is presented as a block diagram in figure 3. A timer signal is produced at the trigger timing by the QCCS.

When a trigger is received from the QCCS, a tick count of the timer records the present time (t_1) and a trigger time (t_2) to compare $t_{12}(=t_1 - t_2)$ with the target time t_0. In the case of $t_{12} < t_0$, the PS timer signal starting from t_2 is in the 'On' state for duration t_0. Otherwise, period t_{12} exceeds t_0, and the output is rendered false.

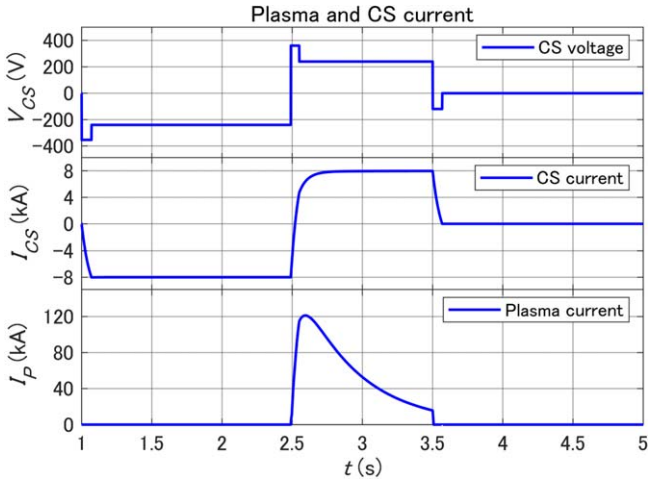

Figure 2. Simulation results for OH scenario. Starting from the top, the panels indicate waveforms of the CS voltage (V_{CS}), CS current (I_{CS}), and plasma current (I_p) from 1 to 5 s.

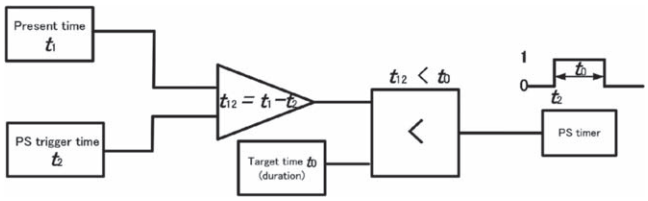

Figure 3. Block diagram of PS timer generator. Present time, t_1, and PS trigger time, t_2, are the input signals. When $t_{12}(=t_1 - t_2)$ is less than t_0, a timer signal with time period t_0 is produced as the output signal.

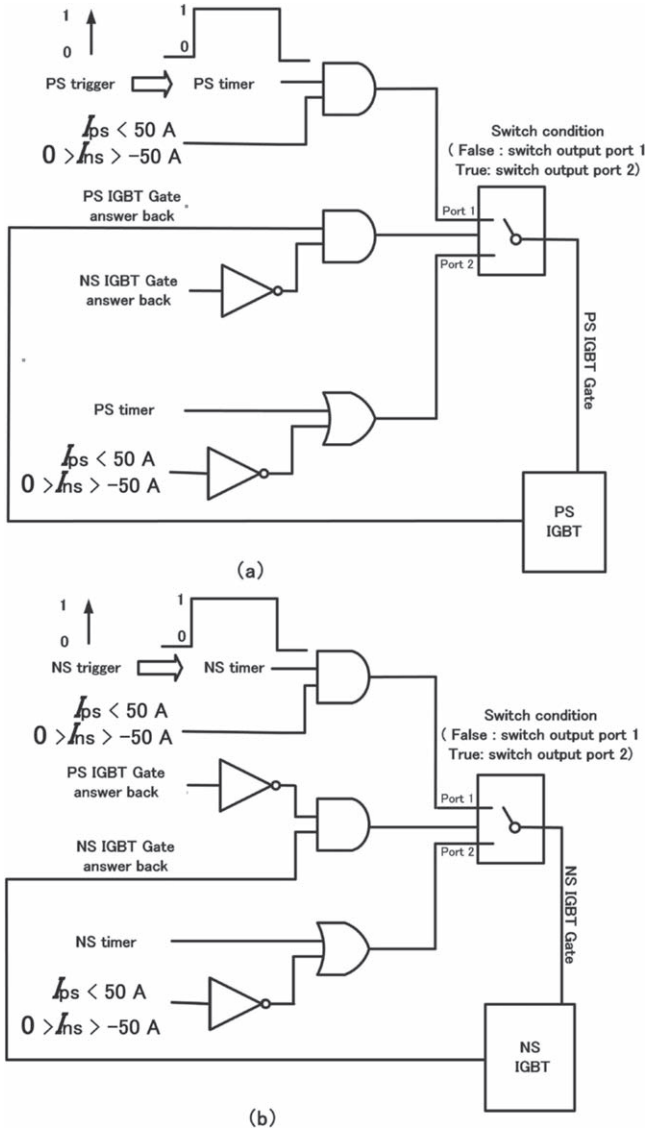

Figure 4. Block diagrams of IGBT gate signals. By determining whether the CS current is less than 50 A, the system generates gate signals for (a) PS IGBT and (b) NS IGBT when a trigger signal is detected by the timer.

(2) Generator of IGBT gate.

The generator of the IGBT gate serves to receive a signal from the CS circuit. This gate signal controls the on-and-off operation of the IGBT stack by analyzing these analog signals. The detailed logic of the IGBT gate is presented in figure 4.

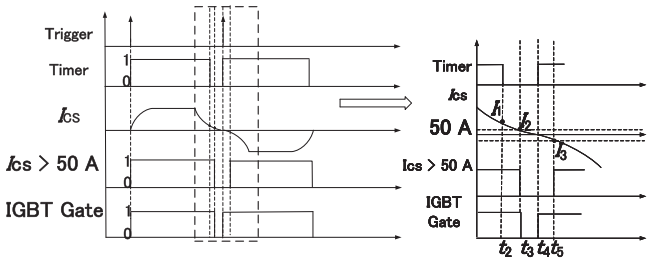

Figure 5. Conceptual waveforms of interlock logics. Starting from the top panel, the trigger pulse, timer logic, CS current signal, logic of $|I_{CS}|$ compared with 50 A, and IGBT gate logic are plotted. Time of the zoomed-in time characteristics of PS–NS switching is shown on the right-hand side.

Figure 4 illustrates a switch connected with an AND gate and an OR gate controlled through the IGBT gate. In the case of PS, if both the IGBTs are in the 'Off' state, the output signal of the switch is produced through Port 1. If the answerbacks from PS IGBT and NS IGBT represent the 'On' and 'Off' states, respectively, then the switch output signal is produced through Port 2.

The AND gate of Port 1 protects the circuit from the arbitrary switching-on of the IGBTs. The FPGA receives the signal value of the CS coil current (I_{CS}) and compares them with 0 A, and accordingly, the analog signal of I_{CS} is transformed into a digital signal. However, completely satisfying this condition of 0 A in the experimental settings is challenging. Instead, a condition for the PS and NS loop current —$I_{PS} < 50$ A and $I_{NS} < 50$ A—is set as 0 A in practical operations. If $0 < I_{PS} < 50$ A and $0 < I_{NS} < 50$ A are not satisfied, or the PS timer signal is true, the IGBT gate signal is supplied through Port 2 to turn on IGBT stack 1. Furthermore, the OR gate protects the circuit from the arbitrary turn-off of the IGBTs. Even if the timer signal is turned to the false state, the IGBT gate is not allowed to turn off before the current satisfies both the conditions of $I_{PS} < 50$ A and $I_{NS} < 50$ A.

Figure 5 plots the conceptual logic waveforms of the IGBT interlock system. The timer signal PS ends at t_2, but the concurrent CS current is $I_1 \geqslant 50$ A. The PS IGBT cannot be turned off until t_3, the time when the condition $I_2 < 50$ A is satisfied. Subsequently, the NS timer starts from time t_4 and $I_{CS} > 50$ A is satisfied from time t_5. These conditions are essential when the PS IGBT is turned off.

2.3. Results of interlock system test

The interlock system is tested, and the corresponding waveforms are plotted in figure 6. The QCCS generates signals of a sequence when the PS and NS are in the working state. At $t = 2.36$ s, the sequence signal of PS ends but I_{CS} is still 6 kA. The interlock system maintains the PS IGBT in the 'On' state until $t = 2.48$ s when I_{CS} decreases to 50 A. In this case, the interlock system protects the PS from switching off with a high current. The NS sequence starts at $t = 2.5$ s, and thus, the interlock can switch on the NS IGBT gate under the condition of $|I_{CS}| < 50$ A.

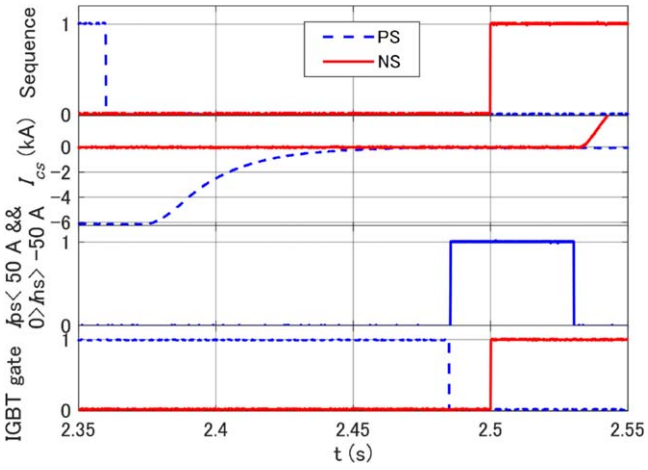

Figure 6. Test results of the interlock system. Starting from the top, the sequence signal generated by the QCCP, CS coil current (I_{CS}), digital logic ($|I_{CS}|$) as true when $|I_{CS}| < 50$ A, and IGBT gate (on/off) signal are plotted.

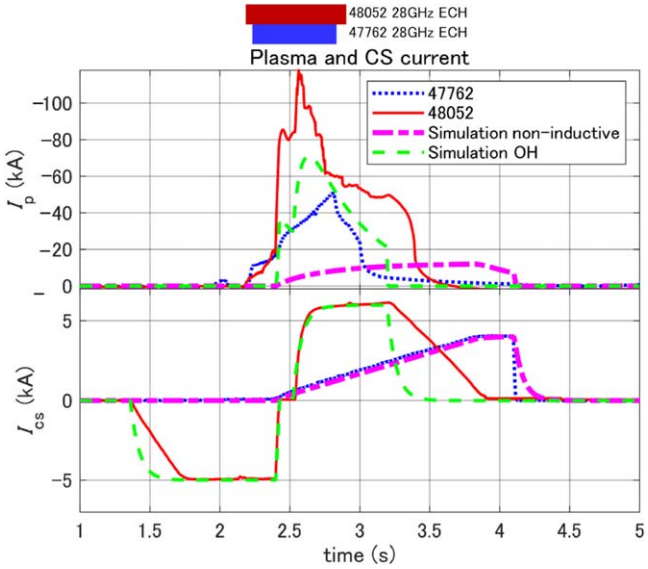

Figure 7. Plasma and CS current of shot Nos. 47762 (blue), 48052 (red) and simulation result (green and purple). Duration of the 28 GHz- ECH is indicated by the bars on the top.

3. Experimental results and discussion

3.1. Plasma current and density

In this study, an experiment was conducted to verify the effect of the upgraded OH and its control system. The results from shot numbers (Nos.) 47762 and 48052 were selected as the representative discharge of a non-inductive current start-up and an OH start-up with double flux swing, respectively. The waveforms of the plasma current and CS current are presented in figure 7.

In this experiment, 28 GHz- ECH was used for ionization and current start-up in both discharges. In shot No. 47762, the plasma current is driven mainly via EC heating. Although the CS current is low, it is necessary for maintaining equilibrium. When the I_{CS} increases to 1.5 kA at 2.8 s, I_P attains a value of

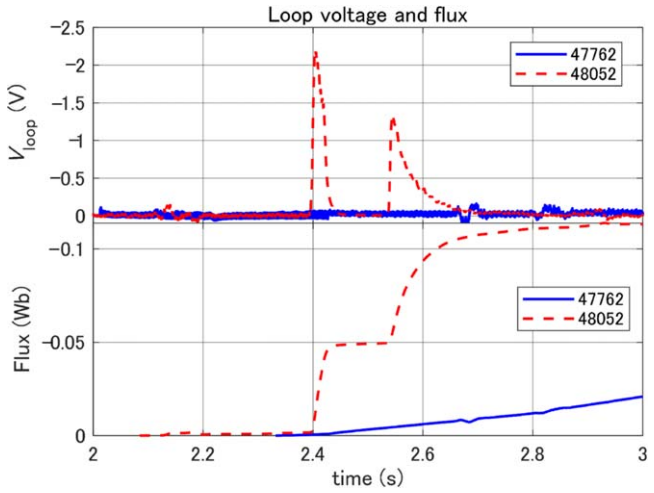

Figure 8. Loop voltage and flux, as calculated using equation (4), corresponding to shot Nos. 47762 (blue) and 48052 (red).

50 kA. In shot No. 48052, the OH power supply with PS and NS is used together in a discharge. At $t = 1.8$ s, I_{CS} approaches 5 kA using the PS. At $t = 2.4$ s, I_{CS} is attenuated to 0 A through the first swing, thereby increasing I_P rapidly, where the 28 GHz-RF also assists in electron heating. In particular, the IGBT switching from PS to NS changes the polarity of I_{CS} at $t = 2.5$ s. The plasma current increases to approximately 120 kA through the second flux swing. The EC heating power is 155 kW and 150 kW in the Nos. 48052 and 47762, respectively.

As the power supplied through the heating is insufficient to maintain such a high current, the plasma current decreases after attaining the peak value. A simulation result of the double flux swing, which has the comparable value of CS current with the experiment, is plotted with dotted green line. The maximum plasma current is about 70 kA that is lower compared with experimental result which is heated by ECH. The simulation result of the non-inductive discharge is plotted by dotted blue line, and it is lower than experimental result because the simulation is only concluded the OH part. In the experiment, non-inductive plasma start-up is mainly realized by ECH. At 2.8 s, EC heating is halted. Thereafter, the plasma current gradually decreases to 0 A because the energetic electrons are confined optimally.

The waveform of the loop voltage, V_{loop}, measured by a flux loop on the CS, is displayed in figure 8. The magnetic flux, Ψ (Wb), generated at the flux loop can be calculated as

$$\Psi = \frac{1}{N}\int V_{loop}\mathrm{d}t, \tag{4}$$

where N (=1) represents the turn of a flux loop. In shot No. 47762, a non-inductive current start-up, the flux consumption only reaches −0.01 Wb at $t = 2.8$ s. Specifically, owing to the double flux swing, the flux approaches −0.045 Wb through the PS and exceeds −0.1 Wb through the NS in shot No. 48052.

The relationship between the flux and the maximum plasma current, corresponding to three The relationship between the flux and maximum plasma current types of start-up methods, is plotted in figure 9. For the non-inductive start-up, the flux swing

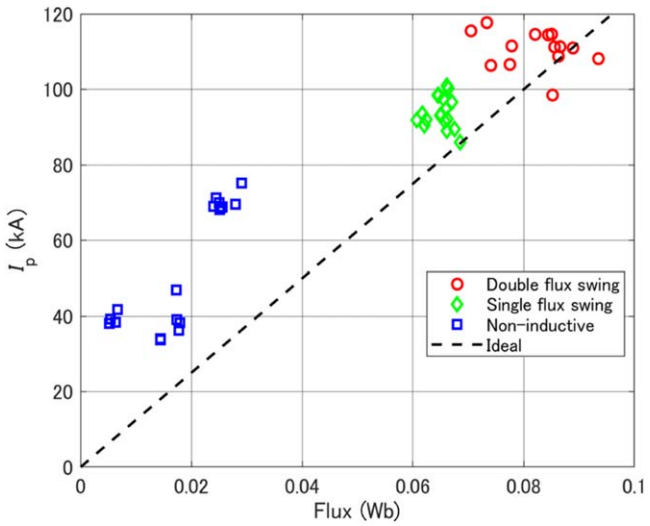

Figure 9. Maximum plasma current with respect to the magnetic flux. Results of non-inductive (blue square), single flux swing (green diamond), and double flux swing (red circle) are plotted. The black dashed-line indicates ideal Ohmic heating, as expressed in equation (5).

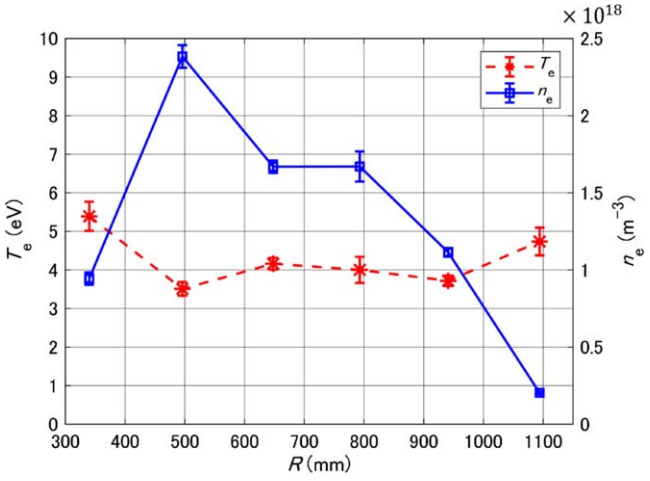

Figure 10. Radical profiles of electron temperature T_e (red) and plasma density n_e (blue) measured through Thomson scattering at $t = 2.6$ s for shot No. 48052.

can merely attain a value of 0.03 Wb, and the maximum plasma current is approximately 60 kA. The single flux swing yields a more significant flux (0.07 Wb) and higher plasma current (100 kA) than those via the non-inductive approach. Notably, the double flux swing yields the maximal flux and plasma current in these three types. Ideally, neglecting the plasma resistance, the as-recorded loop voltage is solely affected by the plasma inductance, L_P, and the mutual inductance, $M_{L,P}$, between the plasma and magnetic flux loop. The relationship between the plasma current and ideal flux (Φ_i), calculated by

$$\Phi_i = (L_P + M_{L,P})I_P, \tag{5}$$

is plotted by the black dashed-line in figure 9. Due to the 28 GHz-ECH, which generates the initial plasma current in advance, the plasma current is greater than the ideal value.

The bulk electron temperature and density measured via Thomson scattering are displayed in figure 10. The horizontal axis represents the tangent radial position. At $t = 2.6$ s, the electron density exceeds the cut-off density of 9.1×10^{17} m^{-3}, which corresponds to the 8.56 GHz EC wave. However, the electron temperature merely attains a value of 5 eV. This low T_e indicates that the energetic electrons absorb both the Ohmic and EC heating power, as demonstrated in a previous experiment [17].

4. Conclusions

OH, through a double flux swing, was applied to the QUEST spherical tokamak. Furthermore, IGBT switching was used to combine the two high-power current sources, and a logical control system with an FPGA was installed in this bipolar power supply. In the experiments, plasma currents were produced through OH. I_P values larger than 100 kA could be obtained stably owing to this new system. Moreover, the high value of I_P, supported the confinement of plasmas. Overly dense plasmas for the 8 GHz range of EC waves were qualified as the target for the EBW experiments. In the future, EBW experiments using 8.56 GHz RF will be conducted in QUEST.

Acknowledgments

The authors thank members of the QUEST group for their technical support. This work was supported by the NIFS Bilateral Collaboration Research Program (Nos. NIFS19-KUTR136, NIFS22KUTR169), Grant-in-Aid for Scientific Research (C) (No. 21K03510), and Collaborative Research Program of the RIAM in Kyushu University.

References

[1] Erckmann V and Gasparino U 1994 *Plasma Phys. Control. Fusion* **36** 1869
[2] Omori T *et al* 2011 *Fusion Eng. Des.* **8** 951
[3] Speth E 1989 *Rep. Prog. Phys.* **52** 57
[4] Hemsworth R *et al* 2009 *Nucl. Fusion* **49** 045006
[5] Tan Y *et al* 2015 *Fusion Eng. Des.* **98–99** 1163
[6] Tao J *et al* 2011 ITER coil power supply and distribution system *Proc. of 2011 IEEE/NPSS 24th Symp. on Fusion Engineering Chicago* (Piscataway, NJ: IEEE) (https://doi.org/10.1109/SOFE.2011.6052201)
[7] Raman R *et al* 2007 *Nucl. Fusion* **47** 792
[8] Raman R *et al* 2009 *Nucl. Fusion* **49** 065006
[9] Kuroda K *et al* 2018 *Plasma Phys. Control. Fusion* **60** 115001
[10] Reusch J A *et al* 2018 *Phys. Plasmas* **25** 056101
[11] Tanabe H *et al* 2017 *Nucl. Fusion* **57** 056037
[12] Takase Y *et al* 2022 *Nucl. Fusion* **62** 042011
[13] Raman R *et al* 2010 *Phys. Rev. Lett.* **104** 095003
[14] Thome K E *et al* 2017 *Nucl. Fusion* **57** 022018
[15] Idei H *et al* 2017 *Nucl. Fusion* **57** 126045
[16] Idei H *et al* 2020 *Nucl. Fusion* **60** 016030
[17] Onchi T *et al* 2021 *Phys. Plasmas* **28** 022505
[18] Shevchenko V F *et al* 2010 *Nucl. Fusion* **50** 022004
[19] Onchi T *et al* 2019 *Fusion Eng. Des.* **146** 2567
[20] Zhang Y F *et al* 2021 *Fusion Eng. Des.* **168** 112362
[21] Li G 2015 *Nucl. Fusion* **55** 033009